Nuclear Reaction Analysis for H, Li, Be, B, C, N, O and F with an RBS Check

W. A. Lanford^{1,*},M. Parenti¹, B. J. Nordell², M. M. Paquette², A. N. Caruso², M. Mäntymäki³, J. Hämäläinen³, M. Ritala³, K. Klepper⁴, V. Miikkulainen⁴, O. Nilsen⁴, W. Tenhaeff⁵, N. Dudney⁵, D. Koh⁶, S. Banerjee⁶, E. Mays⁷, J. Bielefeld⁷, and S.W. King⁷

¹Physics Department, University at Albany SUNY, Albany, NY 12222, USA
2Department of Physics, 257 Flarsheim Hall, University of Missouri–Kansas City,
5110 Rockhill Road, Kansas City, MO 64110, USA

³Laboratory of Inorganic Chemistry, Department of Chemistry, University of Helsinki,
P.O. Box 55, Helsinki FI- 00014, Finland

⁴Department of Chemistry and Centre for Materials Science and Nanotechnology, University of Oslo,
P.O. Box 1033, Blindern, Oslo, N-0315, Norway

⁵Solid State Division, Oak Ridge National Laboratory, Oak Ridge, TN 37831 USA

⁶Department of Electrical and Computer Engineering, Microelectronics Research Center,
University of Texas at Austin, 10100 Burnet Road, Austin, Texas 78758

⁷Logic Technology Development, Intel Corporation, Hillsboro, OR 97124, USA

Abstract: ¹⁵N nuclear reaction analysis for hydrogen is combined with 1.2 MeV deuteron induced nuclear reactions which provide a simultaneous analysis for Li, Be, B, C, N, O and F. The energy dependence of these 1.2 MeV deuteron induced nuclear reactions has been measured and used to correct for the energy loss of the incident deuteron beam in the film being analyzed. After the nuclear reaction analysis is completed, a conventional 2 MeV He RBS measurement is made. Film composition is determined by a self-consistent analysis of the light element nuclear reaction data (both ¹⁵N and deuteron) combined with an RBS analysis of any heavy element (typically Si) present in the film. This composition is used to make RUMP simulations with no adjustable parameters of the complete RBS spectrum. Comparison of this simulated RBS spectrum with the measured spectrum provides a powerful check that there are no major undetected components in the film, and, in some cases, a check that the film has uniform composition vs depth.

Key words: nuclear reaction analysis, light elements, electronic materials

* Corresponding author: wlanford@albany.edu

1. Introduction

The relentless pursuit of Moore's Law in the past decade has been greatly facilitated by a series of new materials and process technologies including such things as strained SiGe, Cu damascene interconnects, low dielectric constant (i.e. low-k) interlayer dielectrics, and high-k gate dielectrics. For Moore's law to live on for yet another decade, still more innovation in the invention and development of new materials will be required. In this regard, materials comprised of low atomic number (*Z*) elements are expected to play a prominent role in the continuation Moore's law for numerous reasons. One early example would be the low-k dielectrics that were originally implemented to replace the higher-k SiO₂ and Si₃N₄ insulating dielectrics utilized in Cu interconnect structures in order to reduce capacitive signal delays and power losses. Typical low-k materials are inorganic-organic hybrids of SiO₂ and a-SiN:H with nominal compositions of SiOCH and SiCNH, respectively. They are commonly formed by adding low *Z* hydrogen and organics to the deposition process of their inorganic component (typically via either plasma enhanced chemical vapor deposition or spin-on deposition methods). The incorporation of hydrogen and organic into the dielectric disrupts the inorganic network structure resulting in a reduction in dielectric constant through the creation of nano-porosity and a decrease in mass density.

The need for increasingly lower k materials has lead the industry to both explore SiOCH and SiCNH materials with increased hydrogen and organic content (up to and greater than 50%) as well as new materials whose network structure consists of other low-Z elements such as B (i.e. SiBN, BN, BCN, and BC)^{4,5} or pure carbon⁶ where reductions in k can be potentially achieved without introducing significant nano-porosity. Low-Z boron and lithium based dielectrics are also of interest for numerous other electronic applications including BN ultra-violet lasers⁷, B₄C neutron detectors⁸, and solid state electrolytes for lithium ion batteries^{9,10}. A need for low-k dielectrics with improved etch resistance to fluorinated chemistries¹¹ and Cu diffusion barrier performance¹² has also driven a recent interest in aluminum oxide and hybrid inorganic-organic aluminum oxide network materials. Yet another low Z element of potential interest in microelectronics is Be with the suggestion that atomic layer deposited beryllium oxide is a candidate high-k dielectric.¹³

In all cases, accurate knowledge of the full elemental composition of these materials (including hydrogen) is needed in order to optimize the properties of such materials. ^{14,15} Secondary ion mass spectroscopy and Fourier-Transform Infra-red spectroscopy are two techniques commonly used in studies of these materials, but these have significant uncertainties due to sputter/ion beam mixing ¹⁶ or optical interference effects. ¹⁷⁻¹⁹ MeV ion beam analysis has proven a powerful procedure for analysis of thin film materials ²⁰. Two widely practiced methods are 2 MeV Rutherford backscattering spectrometry (RBS) ^{21,22} which is good for heavy elements in a lighter element matrix, and nuclear reaction analysis (NRA)²³ which is good for light elements, including hydrogen²⁴.

2 MeV RBS, by far the most widely practiced MeV IBA method, has the key advantage that (for non-crystalline films) given the elemental content, the RBS energy spectrum can be reliably predicted using a program such as RUMP²⁵. This can be done because RBS relies only on well understood physics: conservation of energy and momentum in two-body collisions, the Rutherford scattering cross section,

and energy loss of ions in matter. However, RBS is not very sensitive to light elements because the cross-sections are small and the signals from light elements typically reside on a large background count from the substrate (commonly Si). Hydrogen is so light that there is no RBS signal directly from H but the presence of H reduces the scattering yield (counts/channel) from the other elements in the film.

NRA is complimentary to RBS in that it is sensitive only to light elements and produces no signal from heavy elements in the film. NRA makes use of nuclear reactions between the bombarding ion and atomic nuclei in the film under analysis. The Coulomb repulsion between the bombarding ion and the target nucleus stops nuclear reactions below a bombarding energy called the "Coulomb barrier". This energy increases with the atomic number of the target atom. For ¹⁵N at the energies used here, the ¹⁵N ions are below the Coulomb barrier for all elements except hydrogen. For 1.2 MeV deuterons, the Coulomb barrier limits nuclear reactions to elements below about Al.

The present work combines ¹⁵N induced NRA for H, deuteron induced NRA for Li, Be, B, C, N, O, and F with 2 MeV RBS with to achieve a self-consistent and complete elemental analysis. Examples of recent studies where this approach has been used include: SiCH^{30,31,32,33}, BeO³⁴, and BCH³⁵.

2. Experimental Procedure

All measurements were made on the 30 degree beamline at the UAlbany (SUNY) Accelerator Laboratory. Multiple samples are loaded on a rotating sample wheel, with samples tilted 6 degree from being normal to the beam direction in order to minimize accidental channeling. There is a Si detector ($d\Omega = 4.95$ sr.) located at 170 degrees to the beam direction and a 3" by 3' BGO detector located 2 cm behind the samples. There are no beam-defining slits anywhere near the sample in order to avoid detecting H from slits during the 15 N NRA. A scintillator can be rotated into the beam and the beam spot viewed on a TV. The beam can be focused with a quadrapole lens and directed (or rastered) with electrostatic steerers. This chamber has robust electron suppression, using both electric and magnetic suppression, between the chamber and beamline.

In a typical run, a sample set would be loaded on the wheel and a standard ^{15}N NRA measurement would be made to determine the H content of these films. Many of the films studied have high H contents and some of the H can be lost during the ion bombardment. Hence, a low beam current is used (few na) and the beam is rastered over a \sim 5 mm by 5 mm spot on the sample. Initially, the beam spot position and size is observed on the scintillator; the beam is blocked, and (using the TV image) a sample is rotated into the target position; the beam block is removed and the number of characteristics gamma-rays from the $^{15}N + H \rightarrow ^{12}C + ^4He + gamma-ray$ reaction for a small beam dose (perhaps 0.125 μ C of $^{15}N^{++}$) is measured/counted. This last step is repeated to see if there is significant H loss during a measurement. The ^{15}N beam energy is then changed to probe H at a different depth. This procedure is capable of reliably measuring the H content of even delicate materials, such as polyethylene (although H loss under bombardment is observed). Note, it is important the ^{15}N NRA measurements be made first due to the possible loss of H during the deuteron or He bombardment.

Once the H content measurements on a sample set have been completed, the bombarding ion beam is switched to 1.2 MeV deuteron (actually, 2.4 MeV D_2^+) and the deuteron NRA measurements are made on all samples. Table I gives a list of the stronger nuclear reactions observed on Li, Be, B, C, N, O, and F along with the cross-sections for reactions routinely used in analysis.

Note, in general, an absorber foil is not used in front of the Si detector. Hence, intense deuteron elastic scattering is seen in the low energy region of the spectrum. A typical beam current is 40 na beam for a dose of $5\mu c$, and, under these conditions high count rate issues are not a problem. For samples with significant amounts of high Z elements present, foils in front of the Si detector could be used to range out the D elastic events.

Once deuteron NRA measurements have been completed, 2 MeV He^+RBS measurements are made on all samples, typically running 40 na for a dose of 5 μ C.

3. Establishing differential cross-sections

The number of counts (c) to be observed for a particular nuclear reaction is given by:

$$c = N n (d\sigma/d\Omega) d\Omega$$

where n = number of incident ions, N = number of atoms/cm² in the target, $d\Omega$ = detector solid angle and $(d\sigma/d\Omega)$ is the cross-section. In an analysis, c is measured, and knowing n, $(d\sigma/d\Omega)$ and $d\Omega$, N is determined, i.e. the amount (in atoms/cm²) of a particular element present in the target. However, before this procedure can be used, the cross-sections need to be determined. The cross-sections have been determined measuring counts (c) from targets with known composition. Some of these targets are films composed largely of the element of interest, such as plasma deposited a-BH_x or a-CH_x, with x determined by the ¹⁵N H profiling, and the amount of boron or carbon determined by RBS (really energy loss of the He ions in an RBS geometry). Other films were oxides or nitrides of known composition. The most difficult cases were determining the cross-sections on the lightest elements Li and Be.

The procedure used to determine the cross-section on Be is illustrated in Figure 1 which shows the RBS spectrum recorded for a beryllium oxide film. Overlaying the measured spectrum are two simulations, one assuming only the measured O and H contents and one simulation adding 939 x 10^{15} Be /cm² to the film, with the Be content adjusted to fit the measured spectrum. This is a difficult case because uncertainty in the measured O content adds to the uncertainty in the Be content and because Be has a relatively small stopping power. The uncertainty in the Be and Li cross-sections reported here are accurate to ± 10 percent.

Table I gives the cross-sections used in our deuteron induced nuclear reaction analysis. The uncertainties in these measured cross-sections are ± 5 percent for the elements B, C, N and O and probably for F. The reservation about F is only that we have limited experience in analyzing this element whereas we have analyzed hundreds of film containing (sometimes large amounts) of B, C, N and O.

Note that cross-sections reported here have not been corrected for natural isotopic ratios. Hence, these cross-sections are appropriate for analysis, such as presented here, but, in some cases, are not the correct isotopic cross-sections. For elements with one dominant isotope, such as Be, C, N, O and F, these cross-sections are correct. For other elements (Li and B), for "nuclear physics purposes" the cross-sections reported here would have to be divided by the fractional abundance of the particular isotope.

4. Energy Dependence of Deuteron Cross-Sections

All the cross sections reported in Table I are for a deuteron beam with bombarding energy of 1.2 MeV with films in which the deuterons loose about 20 keV traversing the film. If a film being analyzed has a deuteron energy loss much greater than 20 keV, the cross-sections reported in Table I will not be appropriate if the cross section changes with ion energy. Hence, the energy dependence of the cross-section has been measured, relative to that at 1.2 MeV, simply by reducing the bombarding energy in small steps below 1.2 MeV. These relative cross-sections for C(E) for carbon are shown in Figure 2, along with a linear fit. Corresponding data for all elements are given in Supplementary Material available online at the Journal.

The procedure for correcting the analysis for this energy dependence is as follows. The ¹⁵N and deuteron induced NRA analysis is used to determine the (approximate) light element content of a film and the He RBS is used to determine the "heavy" elements (Al, Si or heavier) content. This approximate film composition is used to determine the deuteron energy loss in the film. With this deuteron energy loss and the energy dependence of the cross-sections given in Figure 2, the compositions are corrected.

In our experience, these energy loss corrections are typically small (a few percent) but not always. An example of where this energy dependence is important is illustrated in Figure 3 which gives the RBS spectrum recorded from a ~1 micron boron carbide on Si film. Also shown in this figure are RBS simulations both before and after energy loss correction. As seen in this figure, after making the energy loss correction, the simulation does a good job of predicting the energy at which the Si signal from the substrate appears whereas before the correction, the prediction is not accurate.

The example in Figure 3 is for a film that is about as thick as can usefully be analyzed using 2 MeV He RBS. We have occasionally analyzed thicker films where we have performed the He RBS analysis at 3 MeV. For such thicker films, this energy correction is even more important.

5. Self-consistent Analysis of the Deuteron NRA and RBS Results in Determining the H Content.

Analysis of the ¹⁵N NRA data to obtain H content requires knowing the stopping power of 6.385 MeV ¹⁵N ions in the target material. That stopping power depends on the elements present in the target, including H. Hence, a self-consistent analysis needs to be done. In particular, an initial guess of the H content is made and used, along with the composition for other elements (from deuteron NRA and He RBS) to evaluate the ¹⁵N stopping power. Using this stopping power and the measured ¹⁵N NRA data,

the H content is determined. Generally this deduced H content is different from the H content guessed at the beginning of the analysis. If this is the case, H content deduced from the ¹⁵N data replaces the initial H content guess and the analysis cycle is repeated until H content used in the stopping power is the same as the H content deduced from the ¹⁵N data. Since the contribution of H to the stopping power is small, experience indicates this process converges very rapidly (3 or 4 cycles) independent of the initial guess for H content.

¹⁵N resonant nuclear reaction data have most commonly been analyzed to give H content in atoms/cm³ whereas deuteron NRA and He RBS naturally gives elemental content in atoms/cm². In order to present analysis from both methods in atoms/cm² requires a modification of the usual ¹⁵N analysis procedure.

The essential point is that the ^{15}N NRA method measures the H content relative to the stopping power from all the elements in the sample. If the analysis results are presented as the ratio of H to the other atoms in the sample, the results are independent of the film density. For example, a ^{15}N analysis of a sample with composition of SiH_{1.00} gives exactly the same H/Si ratio if the film's density in 1 gm/cm³ or 2 gm/cm³ (whereas the H content in atoms/cm³ for the more dense sample is twice that of the lower density film). Hence, one way get the H content in atoms/cm² is to arbitrarily assume a film density, (perhaps $\rho = 1$ gm/cm³) and analyze the ^{15}N data under this assumption, getting H content nominally in atoms/cm³. Next evaluate the elemental content in atoms/cm³ of a one of the other elements (perhaps Si) present in the film, *under the same assumed density*. Multiplying the ratio of H to this other element (perhaps Si) times the content of this other element in atoms/cm², gives the H content in atoms/cm².

An example of the effect of H content on the RBS spectrum is shown in Figure 4. Presented are the measured RBS spectrum and two simulated RBS spectra, one with H and one without. The simulation without H does a poor job. For films containing substantial amounts of H, the H content is essential in simulating the RBS spectrum.

6. Typical Examples

Figure 3-7 show typical examples of this method. In each case, on the right is the deuteron NRA spectrum and on the left is the RBS spectrum with a RUMP simulation, made with no adjustable parameters. Composition of the film is given in the figure captions in the format that B(10256) means a boron content of $10,256 \times 10^{15} \text{ B/cm}^2$. These examples were chosen so as to show at least one deuteron NRA spectrum with peaks for each element Li, Be, B, C, N, O and F.

7. Comments and Conclusion

All three measurements (15 N NRA, D₂⁺ NRA, and He⁺ RBS) are needed for a proper analysis. The deuteron energy loss correction is generally small but, as in Figure 3, can be ~20 percent for a 1 micron film. The need to measure H content in order to simulate an RBS spectrum is demonstrated in Figure 4. This is an example with a relatively modest amount of H (28 percent atomic). Films with 50

percent H (or more) are common (e.g. as in Figure 5), making the effect of the H content on the RBS spectrum even larger than illustrated in Figure 3.

Several hundred samples have been analyzed using the combination of measurements described in this paper and the method has proven to be robust. Indeed, this combination of measurements usually over-determines the film composition. While such over-determination may seem a luxury, from the point-of-view of analysis, such over-determination provides insurance. Comparing an RBS simulation made with no adjustable parameters with the measured spectrum provides a powerful check that no serious errors (or omissions) have been made in the analysis.

8. References

- 1. K. Kuhn, Microelectron. Eng. 88, 1044 (2011).
- 2. S. King, H. Simka, D. Herr, H. Akinaga, and M. Garner, APL Mater. 1, 040701 (2013).
- 3. K. Maex, M. Baklanov, D. Shamiryan, F. Iacopi, S. Brongersma, Z. Yanovitskaya, J. Appl. Phys. 93, 8793 (2003).
- 4. W. Kane, S. Cohen, J. Hummel, B. Luther, D. Beach, J. Electrochem. Soc. 144, 658 (1997).
- 5. T. Sugino, Y. Etou, T. Tai, H. Mori, Appl. Phys. Lett. 80, 649 (2002).
- 6. K. Zagorodniy, D. Chumakov, C. Taschner, A. Lukowiak, H. Stagmann, D. Schmieber, H. Geisler, H. Engelmann, H. Hermann, E. Zschech, IEEE Trans. Semi. Manf. 21, 464 (2008).
- 7. K. Watanabe, T. Taniguchi, and H. Kanda, Nature Mater. 3, 404 (2004).
- 8. A. Caruso, J. Phys.: Condens. Matter 22, 443201 (2010).
- 9. N. Dudney, Interface 3, 44 (2008).
- 10. J. Hamalainen, F. Munnik, T. Hatanpaa, J. Holopainen, M. Ritala, M. Leskala, J. Vac. Sci. Technol. A 30, 1A106 (2012).
- 11. K. Yonekura, S. Sakamori, K. Goto, M. Matsuura, N. Fujiwara, M. Yoneda, J. Vac. Sci. Technol. B 22, 549 (2008).
- 12. P. Majumder, R. Katamreddy, C. Takoudis, Electrochem. Sol. Stat. Lett. 10, H291 (2007).
- 13. J. Yum, T. Akyol, D. Ferrer, J. Lee, S. Banerjee, M. Lei, M. Downer, T. Hudnall, C. Bielawski, and G. Bersuker, J. Vac. Sci. Technol. A29, 61501 (2011).
- 14. E. Andideh, M. Lerner, G. Palmrose, S. El-Mansy, T. Scherban, G. Xu, J. Blaine, J. Vac. Sci. Technol. B 22, 196 (2004).
- 15. S. Gates, D. Neumayer, M. Sherwood, A. Grill, X. Wang, M. Sankarapandian, J. Appl. Phys. 101, 94103 (2007).
- 16. A. Grill, D. Edelstein, M. Lane, V. Patel, S. Gates, D. Restaino, S. Molis, J. Appl. Phys. 103, 54104 (2008).
- 17. S. King, J. Bielefeld, M. French, W. Lanford, J. Non-Cryst. Sol. 357, 3602 (2011).
- 18. S. King, M. Milosevic, J. Appl. Phys. 111, 73109 (2012).
- 19. M. Milosevic, S. King, J. Appl. Phys. 112, 93514 (2012).

- 20. Y. Wang and M. Nastasi Ed., <u>Handbook of Modern Ion Beam Materials Analysis</u>, Materials Research Society, Warrendale, Pennsylvania (2009).
- 21. J. A. Leavitt, L. C. McIntyre and M. R. Weller, page 43-80 in Y. Wang and M. Nastasi Ed., <u>Handbook of Modern Ion Beam Materials Analysis</u>, Materials Research Society, Warrendale, Pennsylvania (2009).
- 22. W.-K. Chu, J. W. Mayer and M. Nicolet, <u>Backscattering Spectrometry</u>, Academic Press, New York (1978).
- 23. G. Vizkelethy, page 125-146 in Y. Wang and M. Nastasi Ed., <u>Handbook of Modern Ion Beam Materials Analysis</u>, Materials Research Society, Warrendale, Pennsylvania (2009).
- 24. W. A. Lanford, page 175-186 in Y. Wang and M. Nastasi Ed., <u>Handbook of Modern Ion Beam Materials Analysis</u>, Materials Research Society, Warrendale, Pennsylvania (2009).
- 25. L. R. Doolittle, Nucl. Inst. Meth. In Phy. Res. B9, 344 (1985).
- 26. S. King, M. French, M. Jaehnig, M. Kuhn, B. Boyanov, B. French, J. Vac. Sci. Technol. B 29, 51207 (2011).
- 27. S. King, M. French, J. Jaehnig, M. Kuhn, B. French, Appl. Phys. Lett. 99, 202903 (2011).
- 28. W. Zhou, S. Bailey, S. Sooryakumar, S. King, G. Xu, E. Mays, C. Ege, and J. Bielefeld, J. Appl. Phys. 110, 43520 (2011).
- 29. S. King, J. Gradner, Microelectron. Rel. 49, 721 (2009).
- 30. S. W. King, M. French, J. Bielefeld, and W. A. Lanford. *Journal of Non-Crystalline Solids*, 357(15), 2970-2983 (2011).
- 31. S. W. King, J. Bielefeld, M. French, and W. A. Lanford, *Journal of Non-Crystalline Solids*, 357(21), 3602-3615. (2011).
- 32. S. W. King, J. Bielefeld, G. Xu, W. A. Lanford, Y. Matsuda, R. H. Dauskardt, N. Kim et al. "Influence of network bond percolation on the thermal, mechanical, electrical and optical properties of high and low-k a-SiC: H thin films." *Journal of Non-Crystalline Solids* 379, 67-79 (2013).
- 33. S. W. King, L. Ross, H. Li, G. Xu, J. Bielefeld, R. E. Atkins, P. D. Henneghan, K. Davis, D. C. Johnson, and W. A. Lanford. "Influence of hydrogen content and network connectivity on the coefficient of thermal expansion and thermal stability for a-SiC: H thin films." *Journal of Non-Crystalline Solids* 389, 78-85 (2014).
- 34. D. Koh, J-H. Yum, S. K. Banerjee, T. W. Hudnall, C. Bielawski, W. A. Lanford, B. French, M. French, H. Li, P. Henry, M. Kuhn, and King, S. W. *Journal of Vacuum Science & Technology B*, 32(3), 03D117 (2014)

35. M. M. Paquette, B. J. Nordell, C. L. Keck, G. Bhattarai, T. D. Nguyen, S. Purohit, and King, S. W. (2015, April). Understanding Field-Dependent Leakage Current Mechanisms in Amorphous Hydrogenated Boron Carbide As a Function of Electronic, Dielectric, and Disorder Parameters. In *Meeting Abstracts* (No. 44, pp. 2285-2285). The Electrochemical Society.

Table I: Deuteron NRA peaks observed for Li, Be, B, C, N, O and F

reaction	excitation ^a	energ y ^b	dσ/dΩ	Figure ^c	C(E) ^d
¹⁴ N(d,p ₇) ¹⁵ N	8.31	1.06	(10^{-27} cm^2)	4	
⁹ Be(d,p ₁) ¹⁰ Be	3.37	1.63		1	
$^{11}B(d,p_0)^{12}B$	0	1.67		3	
19 F(d,p ₁₀) 20 F	3.49	1.69	3.49	7	3.1441*E-2.7727
¹⁴ N(d,p ₆) ¹⁵ N	7.56	1.71		4	
$^{16}O(d,p_1)^{17}O$	0.87	1.77		1,5,6	
¹⁴ N(d,p ₅) ¹⁵ N	7.30	1.94		4	
¹⁴ N(d,p ₄) ¹⁵ N	7.14	2.08		4	
10 B(d,p ₆) 11 B	7.30	2.29		3	
$^{16}\mathrm{O}(\mathbf{d},\mathbf{p}_0)^{17}\mathrm{O}$	0	2.54		1,5,6	
$^{16}\mathrm{O}(\mathrm{d},\!\alpha_0)^{14}\mathrm{N}$	0	2.67	6.55 ^e	1,5,6	-3.4069*E+5.1066
10 B(d,p _{4,5}) 11 B	6.74, 6.79	2.76		3	
¹⁴ N(d,p ₃) ¹⁵ N	6.32	2.80		4	
$^{12}\mathrm{C}(d,p_0)^{13}\mathrm{C}$	0	3.09	93.6	1,3,5,6,7	4.5488*E-4.4463
⁹ Be(d,t ₀) ⁸ Be	0	3.15		1	
¹¹ B(d,α ₂) ⁹ Be	2.43	3.63		3	
¹⁴ N(d,p _{1,2}) ¹⁵ N	5.27, 5.30	3.73		4	
$^9\mathrm{Be}(\mathrm{d},\!\alpha_1)^7\mathrm{Li}$	0.48	3.73		1	
$^9\mathrm{Be}(\mathrm{d},\!\alpha_0)^7\mathrm{Li}$	0	4.00	4.04	1	0.69290*E+0.1418
¹⁰ B(d,p ₃) ¹¹ B	5.02	4.24		3	
$^6\mathrm{Li}(\mathbf{d},\mathbf{p}_0)^7\mathrm{Li}$	0	4.35		6	
⁹ Be(d,p ₀) ¹⁰ Be	0	4.45		1	

10 B(d,p ₂) 11 B	4.44	4.74		3	
$^{11}\mathrm{B}(\mathrm{d},\alpha_0)^9\mathrm{Be}$	0	5.15	2.97	3	1.5927*E-0.9291
$^{13}C(d,p_0)^{14}C$	0	6.02			
$^{7}\mathrm{Li}(\mathbf{d},\alpha_{0})^{5}\mathrm{He}$	0	6.58	4.90 ^f	6	-1.9540*E+3.3419
$^{14}\mathrm{N}(\mathrm{d},\!\alpha_1)^{12}\mathrm{C}$	4.43	6.66	2.26	4	-1.2511*E+2.5058
19 F(d, α_1) 17 O	0.87	7.75			
$^{19}\text{F}(d,\alpha_0)^{17}\text{O}$	0	8.15			
$^6\mathrm{Li}(\mathrm{d},\alpha_0)^4\mathrm{He}$	0	9.15			
$^{14}N(d,\alpha_0)^{12}C$	0	9.75			
$^{10}\mathrm{B}(\mathrm{d},\alpha_0)^8\mathrm{Be}$	0	10.81			

- a. This column gives the excitation energy (in MeV) in the final nucleus.
- b. This column gives the energy of the outgoing particle, calculated using conservation of energy and momentum and the reaction Q-value
- c. This column indicates which of Figures which show peaks for the particular reaction.
- d. C(E) = ratio of cross section at energy E to cross section for E=1.2 MeV deuterons.
- e. Because peaks from $^{16}O(d,p_0)$ and $^{16}O(d,\alpha_0)$ often merge for thicker films, counts from both peaks are summed and the cross section reported is the sum of the cross sections for both peaks.
- f. This is a broad peak. Counts (and cross section) are from an energy region centered on this peak with a total width of 920 keV.

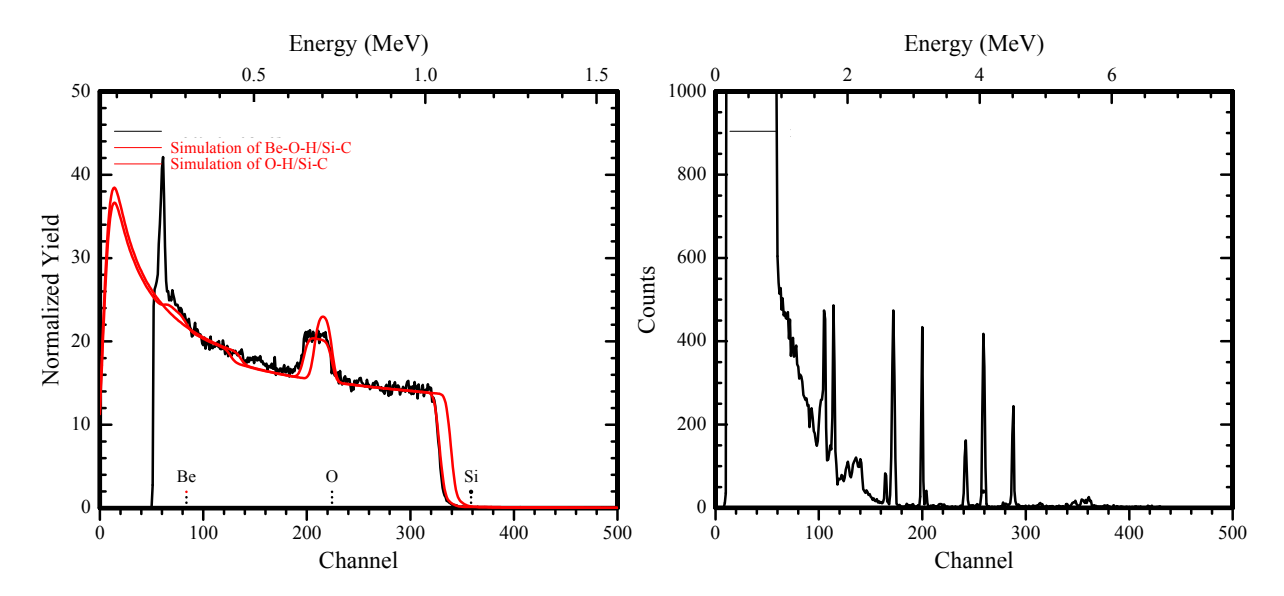


Figure 1: On right is a deuteron NRA spectrum for a "BeO" film on Si. Note the 3 peaks to the right are from Be, the peak at ~channel 200 is from C, and the two peaks between ~channels 160-180 are from O.

On left is the measured RBS spectrum and two simulations, one with O and H determined by NRA but with no Be and one with 939 x 10^{15} Be /cm². Both simulations use 880 x 10^{15} O /cm² and 118 x 10^{15} H/cm².

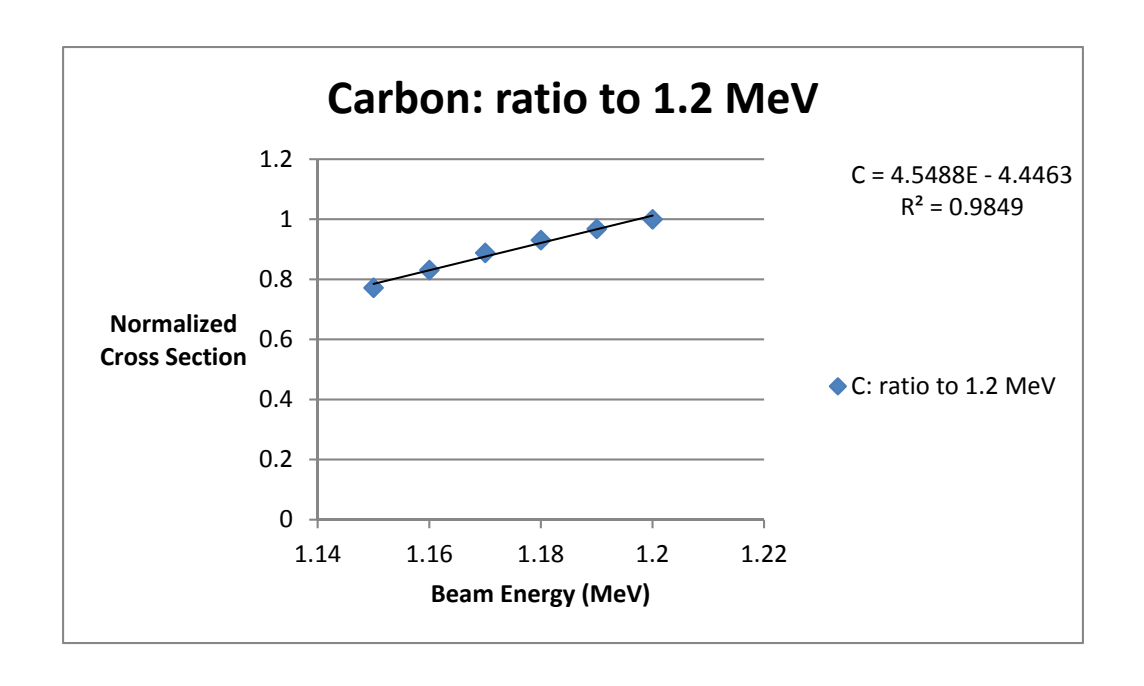


Figure 2: Typical data showing the ratio (C) of the cross-section at beam energy E to the cross-section for deuteron energy of 1.20 MeV for carbon, along with a linear fit to those data. Note, the linear fit has C = 1.0 for deuteron beam energy E = 1.20 MeV. The cross-section energy dependence for all elements is given in Table I. Similar experimental data for Li, Be, B, N, O and F are shown in the Supplementary Material available online at the Journal.

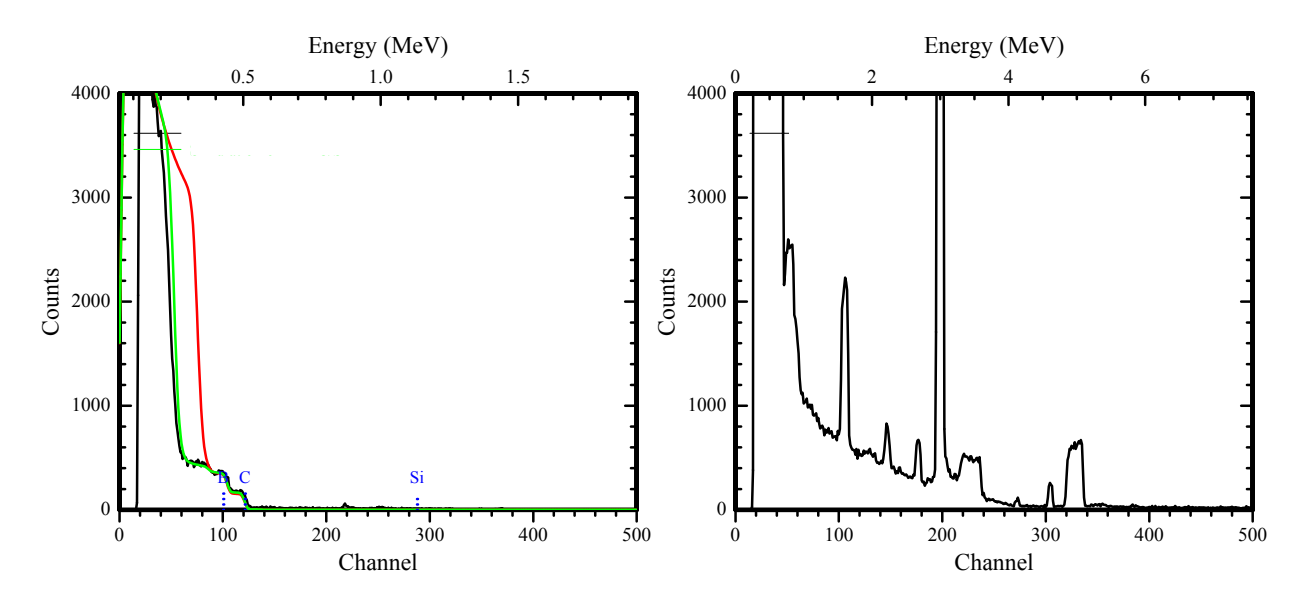


Figure 3: On the right is a deuteron NRA spectrum for a "boron carbide" on Si sample. The peaks used in the analysis are the B peak between ~channel 320-340 and the C peak ~channel 200.

On left is the measured RBS spectrum along with two simulations. One simulation used composition before applying the energy loss correction {B(10256), C(4607), H (118)} and one used the composition after correcting for deuteron energy loss {B(10826), C(5453), H(123)}. Note that the composition before correction badly misses the energy at which RBS for Si in the substrate appears while after correction the predicted energy matches experiment.

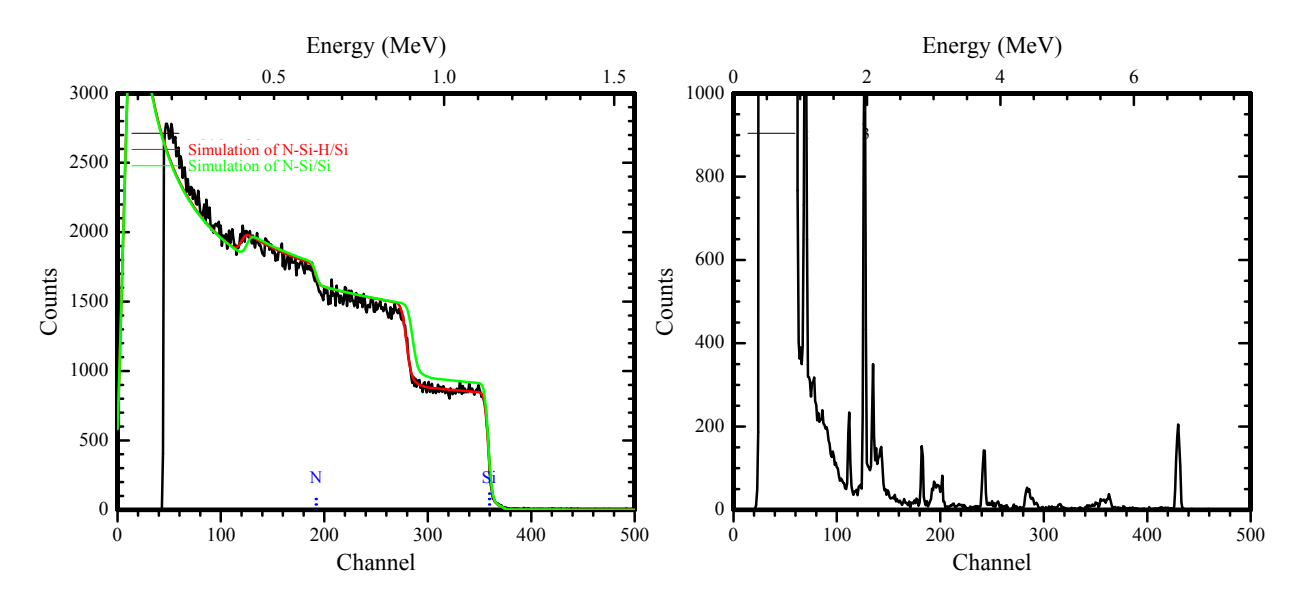


Figure 4: On right is a deuteron NRA spectrum for a silicon nitride film on Si. The peak used for N analysis is in ~channel 430.

On the left is the RBS spectrum measured for this sample along with two simulations. One simulation uses the full composition of the film $\{Si(1674), N(1233), H(1123)\}$. This simulation predicts the data very well. The other simulation uses the same Si and N content but puts the H content to 0. The simulation without H misses the data.

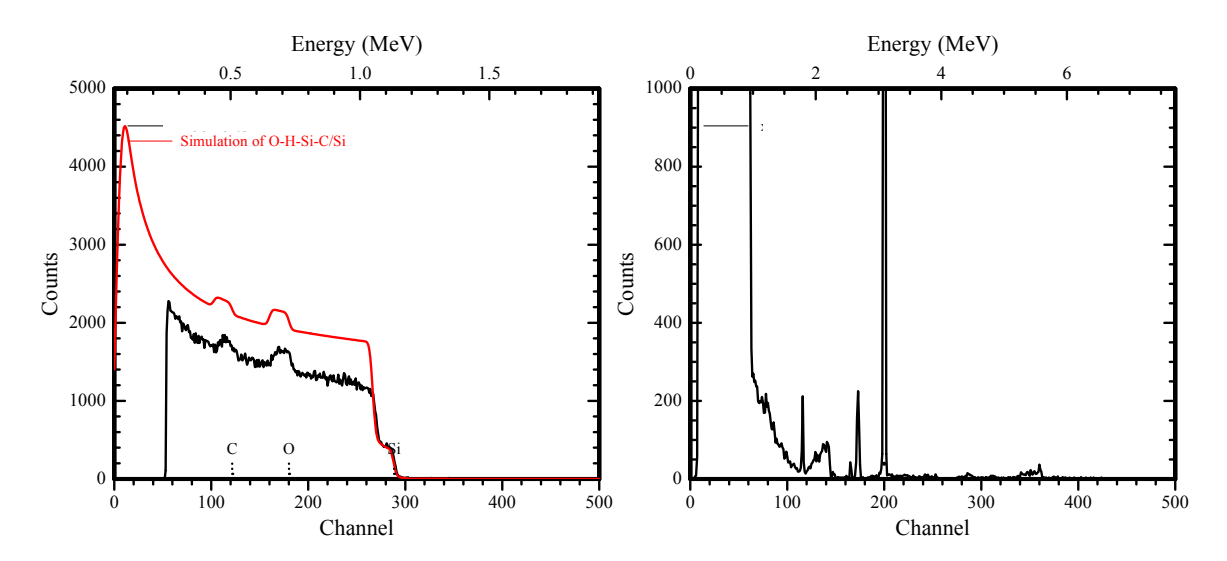


Figure 5: On right is a deuteron NRA spectrum for a SiCOH film on Si. The peak used for C analysis is in ~channel 200 and the peaks used for the O analysis are in ~channels 160-180.

On the left is the RBS spectrum measured for this sample along with a simulation using the composition C(476), O (379), Si (217), H(862) Except for the fact that the simulation does not predict the counts from the Si substrate (due to accidental channeling), this simulation predicts the data very well.

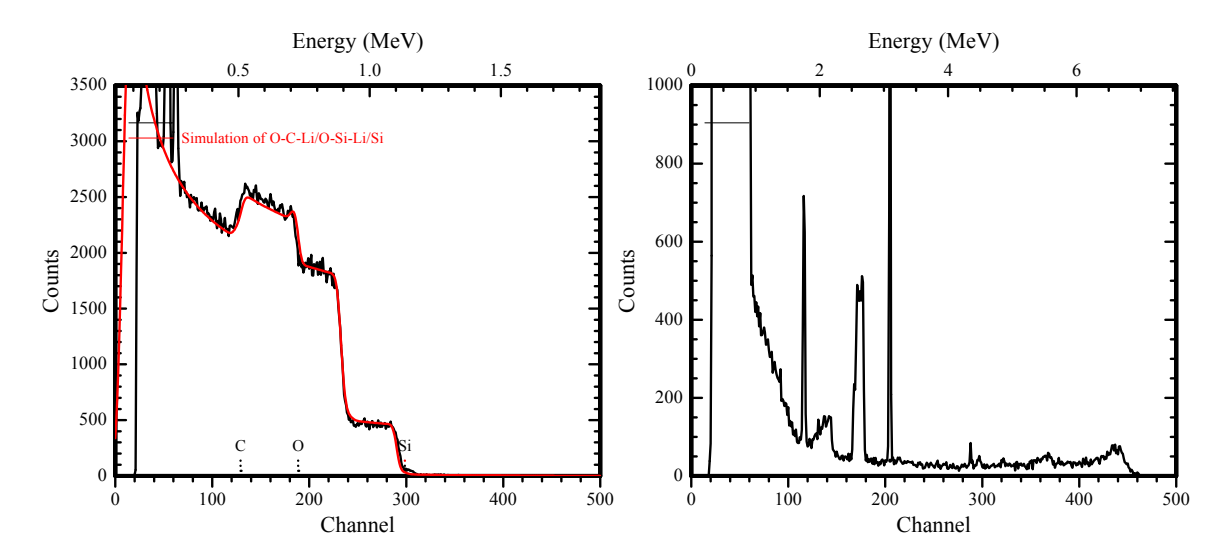


Figure 6: On right is a deuteron NRA spectrum for a SiLiCOH film on Si. The peak used for Li analysis is the broad peak centered at ~channel 440; the peak used for C analysis is in ~channel 204 and the peak used for the O analysis is in ~channels 160-180.

On the left is the RBS spectrum measured for this sample with an overlaying simulation. The simulation assumed a thin layer of Li_2CO_3 (108 x $10^{15}/cm^2$) and a bulk film with the composition Li(1308). O (1752), Si (657)

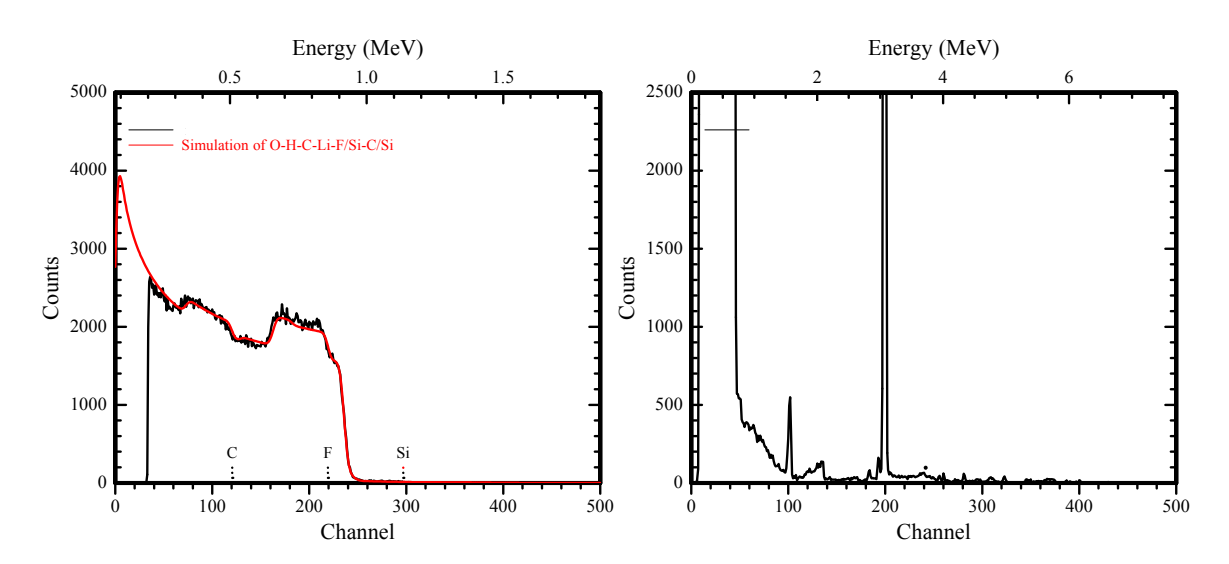


Figure 7: On right is a deuteron NRA spectrum for a CFH film on Si. The peak used for C analysis is in ~channel 200 and the peak used for the F analysis is in ~channel 100.

On the left is the RBS spectrum measured for this sample along with a simulation using the composition C(2060). F (1484), H(280). This simulation predicts the data very well.

Supplementary Material

